Technische Universität Hamburg-Harburg

Institute for Ship Structural Design and Analysis

Project Thesis

On the topic of

Combined FEM – SPH simulations for ice in compression

Author:	Niklas Düchting
	niklas.duechting@tuhh.de
Matriculation Number:	21159368
First Examiner:	Prof. DSc. (Tech.) Sören Ehlers
Supervisors:	M.Sc. Leon Kellner
	M.Sc. Hauke Herrnring

Eidesstattliche Erklärung

Hiermit versichere ich, Niklas Düchting an Eides statt, dass ich die vorliegende Projektarbeit selbstständig und ohne fremde Hilfe verfasst und keine anderen als die angegebenen Hilfsmittel benutzt habe. Die Arbeit ist noch nicht veröffentlicht oder in anderer Form als Prüfungsleistung vorgelegt worden.

_____ _____

Ort, Datum Niklas Düchting

Table of Contents

Nomenclature

Only globally relevant variables and indices are declared in this section. For variables that are not used multiple times the meaning should be clear from the context.

Operators, functions and abstract definitions

f(x)	objective function, field variable
Φ(x)	ansatz-, shape-, trial-, field function
s	displacement
T	temperature
ε	strain
E	Young's Modulus
υ	Poisson's Ratio
ρ	density

Abbreviations

BC	Boundary Conditions
FEM	Finite Element Method
IC	Initial Conditions
IIV	Ice Induced Vibrations
MAT24	Piecewise Linear Plasticity
MAT63	Crushable Foam
ODE	Ordinary Differential Equation
OWE	Offshore Wind Energy
PDE	Partial Differential Equation
SKF	Institute for Ship Structural Design and Analysis
SPH	Smoothed Particle Hydrodynamics
DEM	Discrete Element Method

1 Introduction

The introduction contains the motivation for the research, the State of the Art defining knowledge gabs and an overview on the methodology.

1.1 Motivation

The offshore wind sector shows great potential for Germany regarding the supply of renewable energy. The German Ministry for Economic Affairs and Energy aims to establish 15 GW of Offshore Wind Energy (OWE) until 2030. Especially the Baltic Sea could, due to shallow waters and good wind conditions, be exploited with conventional techniques. Monopiles have shown its reliability in several wind parks in the German bight as well as in the Baltic Sea. Therefore they are especially attractive for further exploration [1].

Sea ice is a potential hazard to offshore structures located in the Baltic Sea. Even in the southern region sea ice with a significant thickness can appear [2]. Adfrozen ice as well as ice floes can lead to high loads on the offshore structure. There are dynamic loads induced by the continuous crushing of bigger ice sheets [3]. Ice Induced Vibration (IIV) needs to be mentioned as a known effect in this context [4].

Due to the topicality of this topic the investigation of sea ice and its interaction with offshore structures provides an interesting research field. For the design it is essential to have an idea of the load cases applied by the environment. The loads applied by sea ice are especially hard to predict as it is a continuously changing and highly complex material. Even under laboratory conditions it is difficult to get repeatable results. Different techniques are used to predict the strength and the behavior of sea ice. Besides empirical formulas, model tests in towing tanks are carried out. Empirical formulas are generated from the experiences gained from field measurements and experiments. Simulations, not yet commercially applied, also use these experiences and formulas to solve the problem numerically.

In this regard, the material model used for the calculations is a major issue. Big efforts are made to find a numerical material model for ice that represents a wide range of measurements and is logical in terms of its physical characteristics. The Finite Element Method (FEM) can be combined with a failure criterion that simply deletes elements when a certain criterion is satisfied. In fact, the material behavior is more complex. Ice could still withstand compression as crushed ice and would not just disappear. A possible solution

is to switch from the grid based FEM to Smoothed Particle Hydrodynamics (SPH), a meshfree particle method. The combined FEM – SPH simulation seems to be a reasonable technique to deal with the physical effects of crushed ice being formed during a compression test.

A compression experiment is usually carried out to investigate the ultimate strength and the behavior of an ice specimen in general. To verify the potential of a combined FEM – SPH simulation, the results of an ice in compression experiment, carried out by the Institute for Ship Structural Design and Analysis (SKF), are used. It is also practical to compare the results of a combined simulation to the results of a simulation without SPH.

The main objective and motivation for this thesis is the numerical investigation on a combined simulation to account for the transformation of solid to crushed ice observed in an ice in compression experiment.

1.2 State of the Art

There are three different techniques to estimate the loads on a structure induced by drifting sea ice. The first technique is the use of design codes or rather empirical formulas. The basis for these empirical formulas are experiences gained through field measurements and experiments. Kellner et al. [5] compared commonly used codes and showed a significant variation for different load cases.

Experiments are indispensable to investigate the behavior of ice in a scientifical manner. Due to the complexity of ice, experiments that use scaled models are facing all kind of inaccuracies and it is difficult to ensure the reproducibility of the results. Different additives are used for the model ice which can differ significantly from sea ice. As a result the scalability of the model scale experiment is becoming an issue [6]. Field measurements are extensive and connected to operational difficulties [7].

Beside the improvement of empirical formulas, the measurements can be used to validate the outcome of a third technique - numerical methods. A selection of ice related simulations covering different simulation methods and material models, is presented in the following:

- The Discrete Element Method (DEM) is used for full scale simulations between ice floes/ridges and a structure. Molyneux et al. [8] investigated this for a vertical cylinder moving into a first year ice ridge. Comparisons have shown that the nu-

merical solution and the experiment are underestimating the ice strength compared to the analytical solution. The author stated scale effects in the experiment and a lack of cohesion between the discrete elements to be the reason for the deviation.

Paavilainen et al. [9] used a combined finite-discrete element method to describe an ice-structure interaction. For this purpose, they introduced a mixed-mode fracture criterion of the finite elements that represents the continuum model or rather the intact ice sheet.

Hilding et al. [10] used a cohesive element method with homogenization for a full scale simulation and compared the results with field measurements. Deviations of the results were attributed to a lack of computational power that allowed only a rather coarse ice model.

- The most established and developed numerical method is the FEM. This method makes a major contribution to the development of ice related simulations.

  A great challenge is the material model that is applied to describe the complex mechanical behavior of ice.

  For instance Moore et al. [11] introduced a user defined material model based on damage mechanics. They took multiple effects of ice in compression into account. Among others they implemented an element deletion criterion based on the amount of damage to describe load drops induced by the extrusion of crushed ice. In following investigations, the authors claimed to improve the deletion criteria by taking physical conditions such as strain rate and temperature into consideration/account. In a simulated collision of an iceberg with a ship side Lui et al. [12] applied a material model consisting of a user-defined failure criterion that is dependent on both the plastic strain and the pressure. In an earlier investigation [13] they introduced the “Tsai-Wu” failure criterion that additionally takes the temperature, salinity and strain rate into account. Alternatively, they adopted a material (MAT078) from the library of the commercial code LS-DYNA to deal with stress waves induced by the erosion of elements. In this material model instead of deleting the element the plastic strain is increased for low and high stresses.

  In LS-DYNA the material “crushable foam” (MAT63) was applied in ice in compression simulations. Gagnon [14] was the first one introducing the foam analogue. Kim [15] took up the idea and implemented a failure criteria depending on the maximum principle stress. The ice characteristics are set by the volumetric strain-stress relationship. Both Gagnon and Kim applied different ice materials in the same simulation to realize a so called high pressure zone (hpz).

Jordaan et al. [16] focused in a simulation particularly on the cyclic loading effects occurring during recrystallisation.

- The SPH method is primary used for hydrodynamic problems. When applied to solid materials it shows advantages over grid based numerical methods for large deformations [17]. The spalling of ice for instance is an event that can be reproduced by a SPH simulation. The spalling effect is particularly distinct for high velocity impacts. A typical application can be the hailstone impact on a structure. Keegan et al. [18] investigated the impact on the leading edge of a wind turbine`s blade.

There are different approaches for the numerical investigation of ice and yet there is no method that can be recognized as superior, universally applicable and reliable. A full-scale simulation can be realized by the DEM predefining the fracture points of the ice. Local effects and the exact physical material behavior can be described by the FEM as it can rely on the most experience. Even though the impact of a hailstone has little in common with the natural crushing of sea ice, it shows that the SPH method is preferably used for events connected to large distortions. In the scope of this work is the investigation of a combined FEM-SPH simulation to account for the change of the physical properties when ice is compressed. For now, in most of the FEM simulations the elements are simply deleted when a certain criterion is met.

1.3 Overview

A clear structure is mandatory for not losing the sight of the objective. The introduction contains the motivation for this thesis and the state of the art of the topic. In chapter 2 the theory necessary to understand the fundamentals of an ice in compression simulation is assessed. Both the characteristics of sea ice and the characteristics of the numerical methods are part of this chapter. The numerical methodology and the numerical studies carried out are presented in chapter 3. It contains the preliminaries, the set-up of an ice in compression experiment, the results and a discussion of these. The conclusion gives the assessment of the author and a possible outlook for further researches on the topic.

2 Theoretical Background

The use of numerical methods has proven its reliability in a wide range of engineering science. The key advantage of these methods in contrast to empirical formulas and model tests is the transferability onto multiple set ups. When applied the behavior of the material needs to be well understood. Especially sea ice is linked with a great amount of complexity. This chapter introduces the central aspects of the thesis.

2.1 Ice Characteristics

Ice exists in an infinite variety in terms of its appearance and physical properties. It depends on how it was formed which in turn depends on the environment and the chemical properties of the liquid. Additives such as salt have a great impact on the formation of ice.

For a comprehensive overview refer to [19–21] which can be seen as a complement to the following text.

2.1.1 Formation of Sea Ice

Under natural conditions in terms of temperature and pressure there is only one crystal structure that is formed when water freezes. The structure of the crystal, known as Ih (h = hexagonal), can be derived from the molecular structure of the water. Two hydrogen atoms are bonded in the liquid state with an angle of about 104° to one oxygen atom. When crystallized the angle is almost the same and still two hydrogen atoms are localized close to the oxygen atoms that are forming a planar hexagon. It is well connected to the other hexagon in one plane. The layers themselves have a weaker connection. Point defects allow an easy travel of dislocations and enable the effect of creeping of the material. Very few molecules, including sodium chloride, do not have the right size to substitute into the ice lattice. Therefore, no matter if made from fresh water or salt water, the ice is chemically the same and the crystal structure is identical.

The formation of ice is fundamentally different when comparing fresh water and sea water. Well known is the anomaly of fresh water and its freezing process. It has its largest density at a temperature of $T = 4°C$. That makes the freezing process fairly simple, the coldest water is at the surface and can start freezing from this point.

Sea water freezes at approximately -1.9°C depending on the its salinity. The water that was cooled down at the surface sinks because of the increase in density. Deeper layers in

the ocean contain more salt and are denser than the sinking water. When the top layer (about 10-20 m) is cooled down to the freezing temperature frazil ice is forming and moves towards the surface. After some other stages [see also Figure 2-1], a solid surface of about 5-30 cm is formed called young ice. The crystals in this layer are unsorted and about 1 mm in diameter. The macroscopic ice-structure consists additionally of fluid (brine) or gas pockets. From this moment the ice is growing from the solid surface layer downwards. Freely drifting young ice is transversally isotropic. The impurity of the ice due to brine pockets and the formation process in general lead to the large deviations of the mechanical properties of sea ice compared to lake ice. Furthermore, the two types of ice show visually a different grain structures. Sea ice is columnar and the one made from fresh water and used for the experiments is granular. In particular the properties of the granular ice are discussed in the following section.

Figure 2-1: Intermediate stage during the formation of sea ice [22]

2.1.2 Mechanical Properties of Ice

Under laboratory conditions the mechanical properties of pure polycrystalline ice are described in the following. A closer look is taken at certain effects and the main ice characteristics are derived.

In general ice shows two different types of behavior when loaded:

I. Viscous behavior resulting in creeping and final collapse
II. Brittle behavior resulting in fractures

Temperature, loading rate and confinement play an essential role regarding these two types of behavior. Generally, ice behaves brittle when loaded rapidly. Figure 2-2 shows the strain-stress behavior for different strain rates for ice in compression. In the following more detail is put into both characteristic ice behaviors.

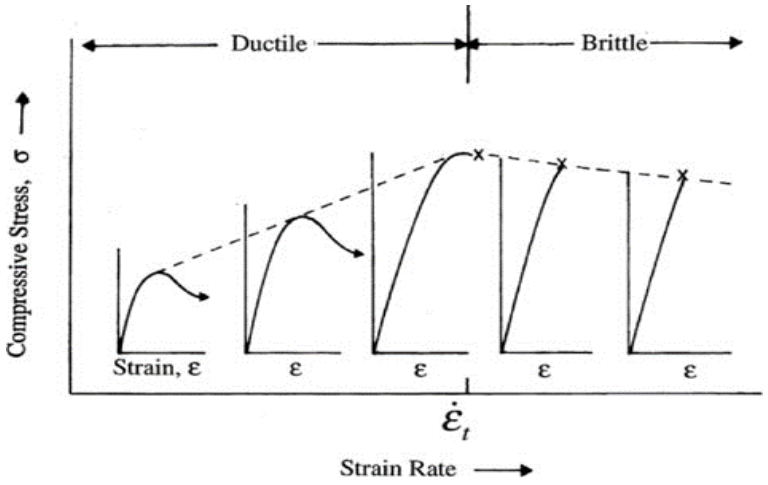

Figure 2-2: Compressive stress-strain relations for different strain rates [21]

There are different stages when observing the ductile also called continuum behavior (I.) of ice. The graph in Figure 2-3 gives the strain versus stress of an isotropic granular ice under constant applied stress. At the beginning an instantaneous strain can be observed (too small to plot). The corresponding Young's Modulus (E) is given in a range between 5 to 9.5 GPa depending on the porosity. The Poisson's Ratio (ϑ) of pure ice for elastic strain is given as 0.33 ± 0.03 in the literature [19]. The next stage is the primary creep which is grain size dependent and shows a continuously decreasing creep rate. The characteristic of the secondary creep is an almost constant creep rate. It was found to be independent on the grain size. Tertiary creep only occurs under relatively high temperatures. It distinguishes by an unstable increase of the strain rate usually caused by the formation of macrocracks and the dynamic recrystallization [21].

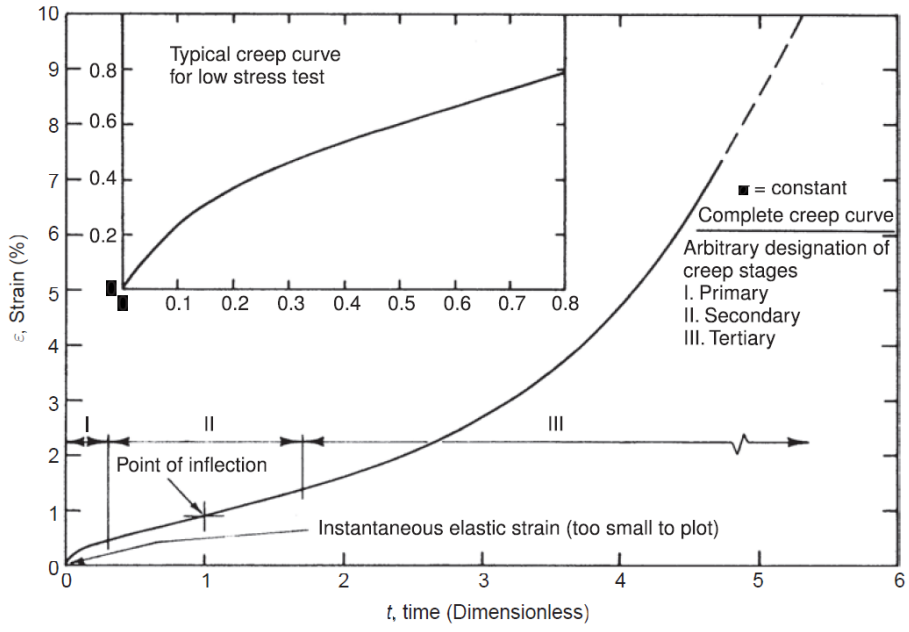

Figure 2-3: Creep curve of isotropic granular ice [21]

The material exhibits under certain circumstances, mainly depending on the strain rate, a brittle behavior (II.) instead of the ductile behavior. It is difficult to define brittle failure strength because it is extremely depended on several factors like the number of impurities, damage, ice temperature and confinement. The distribution of the impurities is stochastic and therefore especially tough to control in the experiment. The main reason for brittle behavior is the strain rate qualitative shown in Figure 2-2. When ice is loaded rapidly creeping or rather the process of dynamic recrystallization is disturbed. As a result, macroscopic cracks develop easier. Ice has its peak of the strain rate at roughly $10^{-3}s^{-1}$, implying that from this point only little creeping is observed. The maximum strain given by more than 1% [19] and the lower temperature are factors which favor the brittle behavior. The values given are reference values that are not necessarily sufficient conditions.

The characteristic strength of the pure ice must be adjusted downwards when looking at sea ice. The main difference are brine pockets enclosed in the structure of sea ice. These pockets cannot support shear stress and cause local stress concentrations. The stress for instance is adjusted by the given brine volume [19]. The compressive strength is primarily dependent on loading rate, temperature and confinement. Typical values given by Timco et al. range from 0,5-5 MPa [20]. Petrovic gives values for the compressive strength of 5-25 MPa [23].

A simple experiment realized by the SKF institute to examine the behavior of the ice material is by compressing an ice cylinder over a large range of strain rates. It generates the basis to the experiment described in section 3.2. Figure 2-4 shows a typical set-up for a compression test. A challenge is the reproducibility of the ice specimens in terms of their mechanical properties. For this purpose impurities and grain sizes simulated by pre-crushed fresh water were studied among others [24]. The compressive strength measured correspond to the values given by Petrovic [23].

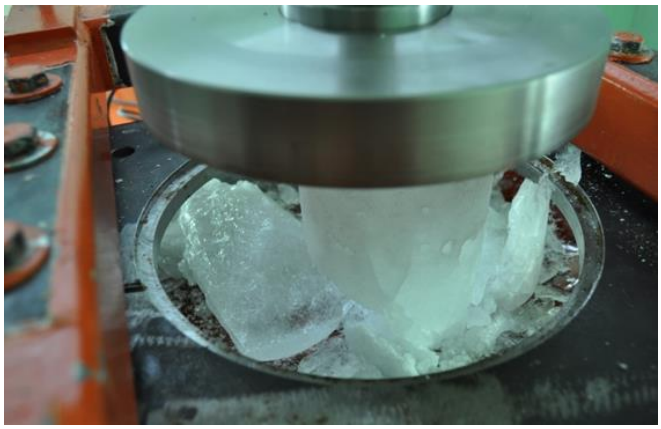

Figure 2-4: Uni-axial compression test

2.2 Numerical Methods

A numerical method aims to reflect or rather simulate the reality. The domain of a physical process described by differential equations is therefore discretized to fit into the scheme of the simulation method. This discretization is mainly dependent on the computing power that can be provided. With increasing numerical power, more realistic models can be created. Numerical methods that were only applied in certain niches now serve multiple purposes where other probably more established methods are facing natural limits. One of these innovative methods is the SPH, originally developed to astrophysical problems and now applied for a wide range of simulations dealing with fluid and solid materials [25, 26].

Section 1.2 underlines that most of the numerical investigations on ice-structure interactions are based on or are related to FEM simulations. This is representative for the simulations carried out in engineering. The FEM is the most established method. Even though the FEM can rely on such an extensive experience it is not excluded from weaknesses such as dealing with large deformation [25]. To comprehend the advantages of a meshless method over the gridbased method, this section serves as an introduction to the SPH method. The FEM method is only briefly explained as there is plenty of literature offering insights to this method [26, 27].

Several commercial FEM programs are established in the market. LS-DYNA is one of them with its origins in the mid-seventies [28]. Because of its strength in highly dynamic simulations and several implemented meshfree methods such as SPH it is suitable for this purpose. Due to practical reasons, the following explanations are related to the way the methods are implemented in the code of LS-DYNA.

2.2.1 Finite Element Method

FEM is furthermore referred to as the classical or conventional method. The FEM has proven its benefits among others due to the increase of the available computational power. In the following, a brief introduction is given.

A Partial Differential Equation (PDE) is assumed that represents the characteristics of a system. Finding an analytical solution for a PDE is often not possible due to its complexity. The idea is to approximate the system by implementing an ansatz (also called shape or trial function), consisting of linear independent equations and solving the weak form of the PDE.

Looking at practical problems it is hard to find only one global ansatz. As the name already suggests the conventional method is breaking a system into finite elements defined using a certain number of nodes. The conus in the following simulation for instance consists of a mesh of 8-node hexahedrons [28]. Another possible shape for 3D elements could be the tetrahedron. The PDE is solved for the nodes in which only one ansatz function is unequal to zero. For nonlinear problems, as in this case dealing with a nonlinear material behavior of ice the solution of the PDE is only iteratively solvable. The global solution is calculated by solving a linear system of equations that contains the boundary conditions of the system. Between the nodes the values are being interpolated. This does not imply having the exact value at the node. The accuracy of the solution is among other factors dependent on the mesh and the ansatz function. However, both - the refinement of the net and the increase of the polynomial degree of the ansatz function – result in an increase of the computational effort [27]. In order to solve dynamic problems, a time integration process is needed. The LS-DYNA default is an explicit time integration scheme. Meaning that in contrast to the implicit time integration scheme only the previous time steps are considered for calculating the current. The time step size (Δ_t) is calculated as a function of a characteristic length (L_e) of an element, the adiabatic sound speed (c) and the bulk viscosity. The sound speed for elastic materials can be written as a function of the density (ρ) and the Young's Modulus (E): $c = \sqrt{\frac{E}{\rho}}$. The time step must be less than the time it takes for a sound signal to travel through an element. For strain rates equal or higher than zero the bulk viscosity coefficient becomes zero and the formula simplifies to the following [28]:

$$\Delta_t \leq \frac{L_e}{\sqrt{\frac{E}{\rho}}} \tag{2.1}$$

There are several limitations of the FEM. These limitations are primarily related to the mesh dependency. The creation of a suitable mesh can be time consuming. With the increase of available computational power, this process is becoming a major time factor in a simulation compared to the calculating time. Furthermore, the FEM has difficulties handling large deformations. Large element distortions can only be treated by complex remeshing. The breakage of a material is furthermore difficult to simulate because the FEM is based on continuum mechanics. Instead of separating the finite elements can only be eroded completely. [25]

For a comprehensive overview please refer to [26].

2.2.2 Smoothed Particle Hydrodynamics

Smoothed Particle Hydrodynamics (SPH) is a meshfree, Lagrangian, particle method. It was originally developed in 1977 to solve astrophysical problems [29, 30]. Nowadays, grid-based numerical methods such as the FEM are already far more developed and continuously applied. Nevertheless, the natural weaknesses of the conventional methods could not be ignored. Around 1990 researches found the SPH method to be a practical alternative. The applications were focused on fluid dynamics, followed by all kinds of mechanical problems. Basically, everywhere large deformations occur such as in the metal forming process, the application is conceivable. Today SPH is a mature method which is implemented in several commercial codes [31].

The absence of the mesh is the main difference compared to the conventional method and requires a new calculation method. The PDEs are not solved at the nodes of the elements but on the particles, which are not strictly connected. In the following, the SPH method and its implementation in LS-DYNA is introduced. Special attention is paid to the application to solid mechanic problems. The fundamental equations will be discussed in section 2.2.2.2.

The following derivations are based on: [25, 28, 31].

2.2.2.1 Basic Idea and Essential Formulations

The term “Lagrangian”, is one of two ways to handle the equation of motion. In contrast to the “Eulerian description”, for which a particle in a certain area is observed, the reference frame is attached to the material point. It is preferably used in solid mechanics because the convective term in the PDE can be avoided. In case of a FEM or rather grid-based methods this description implies that the grid is attached to the material. Naturally this results in relative motion of the nodes and a deformation of the mesh. For extremely distorted meshes the accuracy of the solution decreases or even terminates with an error. A possibility is remeshing the problem domain and integrating the Eulerian description. In many cases this creates difficulties and as a logical consequence a Lagrangian numerical method which is not dependent on a mesh would be a superior solution.

The procedure of the SPH method is comparable to all the other numerical methods. To emphasize the differences the basic procedure is divided into the following sections:

I. Formulation of the governing equations with Boundary Conditions (BC) and/or Initial Conditions (IC)
II. Discretization of the problem domain by a set of particles
III. Numerical discretization
    A. Kernel approximation
    B. Particle approximation performed at every time step
IV. Numerical method is applied to solve the PDE/ODE

In more detail, the points that distinguish SPH from FEM:

II. The system is discretized by particles with individual masses. Compared to the FEM the connection between the particles, which describe the problem domain, does not have to be predefined. Nevertheless, there are some recommendations regarding the distribution of the particles. LS-DYNA advises the user to choose an arrangement that is as regular as possible and does not contain large variations. An example is given for the discretization of the profile of a cylinder shown in Figure 2-5. In this case “Mesh 1” is preferred [28].

Figure 2-5: SPH mesh requirements [28]

Beside defining the particles according to the geometry, it is common practice to use the mesh generation algorithms of the FEM. The particles are deployed in the mesh cell using the geometric or the mass center as a reference. Placing the particles at the nodes can often provide a smoother surface but is not always available in commercial programs. The distribution using the mesh generation methods lead to the conclusion that it can only be as good as the mesh itself. For a combined FEM-SPH simulation there is no other way but to use the predefined mesh because the SPH particles shall be generated out of eroded elements. LS-DYNA can adapt 1,8 or 27 discrete elements all arranged around the geometric center of the solid element. The distribution of the second option is shown in Figure 2-6.

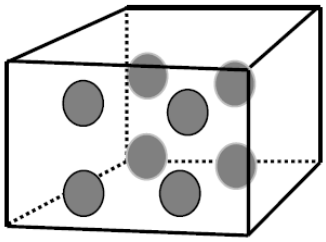

Figure 2-6: Distribution of discrete elements [28]

III. Obtaining an analytical solution for the governing equations of the system defined in (**I**) is usually not possible. A numerical solution requires certain simplifications starting with the discretization of the problem domain (**II**). The numerical discretization is separated into the kernel approximation (**III.A.)** followed by the particle approximation (**III.B.)**.

III.A. The kernel approximation can be imagined as the frame for an approximation of a field variable (*f(x)*) in an integral form. This variable is valid for one point, defined by a three-dimensional position vector x. This point is usually the position of a particle. The exact value is given for the following integral

$$f(x) = \int_{\Omega} f(x')\delta(x - x')\mathrm{d}x' \tag{2.2}$$

where Ω is the integral volume that contains x and $\delta(x - x')$ is the Dirac delta function defined as

$$\delta(x - x') = \begin{cases} 1 & x = x' \\ 0 & x \neq x' \end{cases} \tag{2.3}$$

The delta function is substituted by the smoothing/kernel function ($W(x - x', h)$). This function considers that the problem domain is discretized with a finite number of particles. For the approximation it is sufficient to take several particles into account that are defined by the smoothing length h. The smoothing length defines a support/influence domain of the particle. To maintain an almost equal number of particles within the support domain, *h* is variable in time and space. In addition to that, the smoothing function should be a centrally peaked function. There are different criteria which are affecting the choice. A common (also in LS-DYNA) used function is the cubic B-spline that is similar to the Gaussian function and is defined as

$$W(R,h) = a_d * \begin{cases} 1 - \frac{3}{2}R^2 + \frac{3}{4}R^3 & for\ |R| \leq 1 \\ \frac{1}{4}(2 - R)^3 & for 1 \leq |R| \leq 2 \\ 0 & for\ 2 > |R| \end{cases} \tag{2.4}$$

Depending on the space dimension $a_{dimension}$ becomes $a_1 = \frac{1}{h}, a_2 = \frac{15}{7\pi h^2}\ or\ a_3 = \frac{3}{2\pi h^3}$. R is the relative distance between two points/particles defined as $R = \frac{|x-x'|}{h}$. The function has a weighting effect since particles depending on the geometric distance have a different impact on the field variables and is therefore monotonically decreasing. The smoothing function W should satisfy the following conditions:

The first condition states the integration of the smoothing function

$$\int_{\Omega} W(x - x', h)\mathrm{d}x' = 1 \tag{2.5}$$

The second condition states that W becomes the delta function or rather the function value when the smoothing length approaches zero

$$\lim_{h\to 0} W(x - x', h) = \delta(x - x') \tag{2.6}$$

The last condition defines that particles outside the smoothing length(κh) are not considered

$$W(x - x', h) = 0 \; when \; |x - x'| > \kappa h \tag{2.7}$$

A simplification exists for the derivative of the integral form of the kernel function which leads to the following equation

$$\Delta f(x) \geq -\int_{\Omega} f(x') * \Delta W(x - x', h) \mathrm{d}x' \tag{2.8}$$

It should be noted that the simplification only applies when the support domain does not intersect with the problem domain.

III.B. The particle approximation can be visualized in Figure 2-7. The sketch shows a finite number of particles within a circular support domain with a radius of κh_i, within a problem domain.

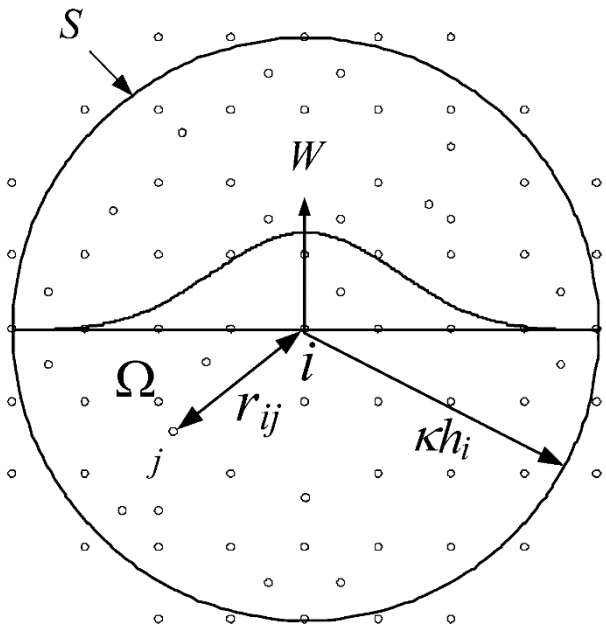

Figure 2-7: Particle approximation and the support domain [17]

The integral form of the kernel approximation can be converted to the discretized form consisting of a summation over the particles in the support domain. For this purpose, the infinitesimal volume dx' is replaced by the finite volume of a particle ΔV_j. The integral representation can now be written in the discretized form

$$f(x_i) = \sum_{j=1}^{N} \frac{m_j}{\rho_j} f(x_j) W(x_i - x_j, h) \tag{2.9}$$

Note that ΔV_j is replaced by the relation of mass and density given as $\frac{m_j}{\rho_j}$. In summary Equation (2.9) approximates the value of a function at a particle i by a weighted average of the particles in the support domain. Because of the introduction of the density in the equation above the method is preferably used in hydrodynamic problems. Special treatments are required when applied to solid mechanic problems. If the smoothing length varies, particles may influence each other only in one direction. This is a violation of Newton's Third Law and is solved by taking a mean value of the corresponding smoothing lengths.

The sorting of the particles as seen in Figure 2-7 is performed in every time step. Therefore, the method can handle extreme and dynamic deformation. This is what makes the method "adaptive".

IV. The particle approximation produces a set of Ordinary Differential Equations (ODE) which are only dependent on time. ODEs can be solved using an explicit integration algorithm. This enables a fast time stepping. The time step size for the SPH method in LS-DYNA is determined by the following equation

$$\Delta t = C_{CFL}\mathrm{Min}_i\left(\frac{h_i}{c_i + \vartheta_i}\right) \tag{2.10}$$

Where c_i is the adiabatic sound speed, C_{CFL} is a numerical constant, ϑ_i is the velocity of the particle and h_i is the smoothing length.

2.2.2.2 Fundamental Equation

The following derivations are based on Benz et al. [32] - introducing a SPH code that is suitable for solid mechanics applications.

Two fundamental equations are now exemplarily implemented into the above described SPH framework. The basic equations presented are the mass (2.11) and the momentum (2.12) conservation

$$\frac{\mathrm{d}\rho}{\mathrm{d}t} + \rho * \frac{\partial}{\partial x^\alpha} * v^\alpha = 0 \tag{2.11}$$

$$\frac{\mathrm{d}v^a}{\mathrm{d}t} = \frac{1}{\rho} * \frac{\partial}{\partial x^\beta} * \sigma^{\alpha\beta} \tag{2.12}$$

Where $\frac{\mathrm{d}}{\mathrm{d}t}$ is the Lagrangian time derivative, ρ is the density, v is the velocity, σ is the stress tensor and α, β are the space indices. The SPH formulation can be derived by multiplying the weighting function W. The conservation equations are solved using the weak form. A possible formulation of the mass conservation is called the symmetric form

$$\frac{\mathrm{d}\rho_i}{\mathrm{d}t} = -\sum_{j=1}^{N} m_j * \left(v_j - v_i\right) * \frac{\partial W_{ij}}{\partial x_i^\alpha} \tag{2.13}$$

And respectively the conservation of the momentum

$$\frac{\mathrm{d}v_i^{\alpha}}{\mathrm{d}t} = \sum_{j=1}^{N} m_j \left(\frac{\sigma_i^{\alpha\beta}}{\rho_i^2} + \frac{\sigma_j^{\alpha\beta}}{\rho_j^2} \right) * \frac{\partial W_{ij}}{\partial x_i^{\beta}} \tag{2.14}$$

2.2.2.3 Summary

Figure 2-8 shows what is happening during one time step. The integration cycle starts with the initial position and velocities. The basis for the following calculations is the definition of the influence domain by the smoothing length. Afterwards the field variables can be solved. Forces, contact conditions and accelerations can be derived, yielding updated positions and velocities. From displacements comes strain, from strain comes stress and the cycle is repeated. Using an explicit time integration allows access to an extend time history of all variables.

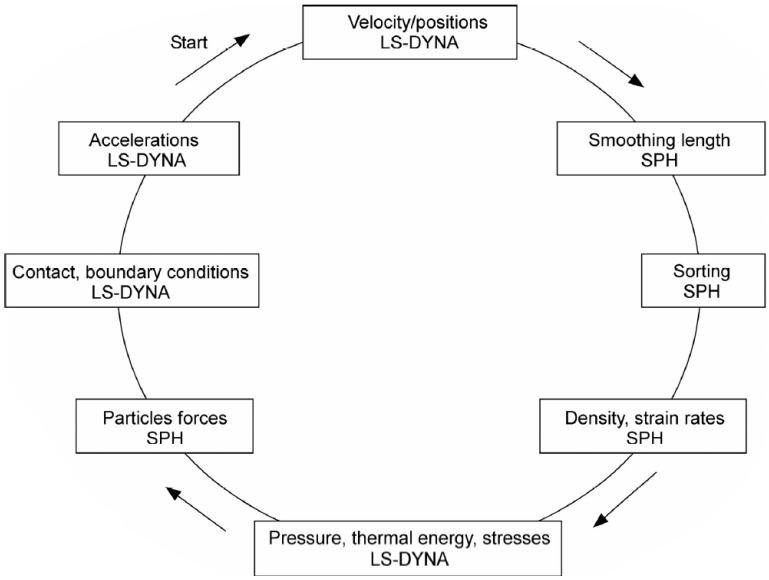

Figure 2-8: SPH calculation cycle [28]

Due to its adaptive characteristics the SPH method will always yield some results. For this reason, the user is particularly advised to verify the outcome. Under certain circumstances the method suffers from boundary inaccuracy and tensile instability [31]. When applying the SPH method the balance between the advantage of adaptivity, the handling of large deformations, accuracy and efficiency should be investigated.

The advantages and disadvantages of both the SPH and the FEM are finally presented

SPH	FEM
+ managing large deformation	+ less computational effort
+ meshless method	+ more expertise
+ discretization of complex geometries	+/- defined influence domain
+/- adaptive character	- dependency on the mesh
- large computational effort	- managing large deformations
- boundary inaccuracy	
- tensile instability	

With a combined FEM and SPH simulation the benefits of both methods could possibly be exploited at the same time.

3 Numerical Studies

This chapter captures the detailed approach of the numerical studies carried out in the course of the project thesis. The first section deals with preliminary considerations with the use of simplified models. In the second section the experiment, which is to be simulated, is introduced. Furthermore, the discretization and Boundary Conditions (BC) used for the final simulations are discussed. In the following two sections the results of the final simulations are presented and discussed. All simulations are performed with LS-DYNA. The following sections refer to the theory and user's manuals [28, 33, 34] unless otherwise stated.

The simulation provides an impression of what can be achieved by assessing the practicability of a combined SPH-FEM simulation. In Figure 3-1 the schematic of the combined simulation is displayed. The basis is a FEM model which contains a failure criterion and a solid to SPH option. The idea is to generate a particle phase named crushed ice from the failed solid phase called ice.

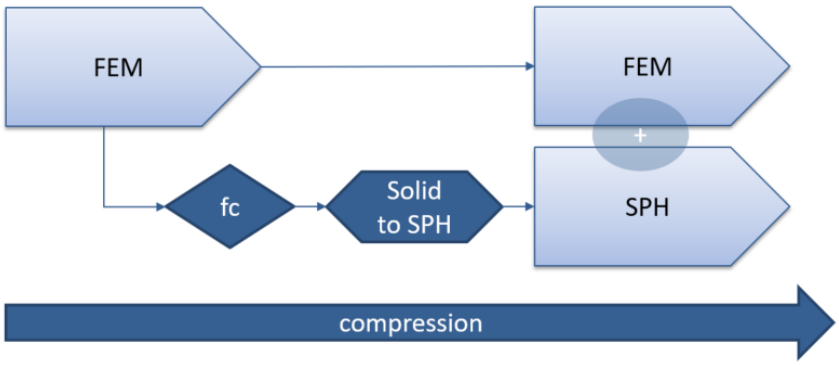

Figure 3-1: schematic of the solid to SPH option

3.1 Preliminaries of the Numerical Model

This section gives insight into the procedure. It states the main decisions and simplifications made during the process of developing the numerical model. The approach is rather practice-oriented and based on trial and error.

The numerical model is developed in LS-DYNA. The dynamic problems are solved using an explicit time integration scheme. For more details please also refer during the following derivations to section 2.2.

3.1.1 Material Model

The numerical model can only be as accurate as the applied material model. Much effort was put into finding a suitable model for the complexity that ice offers. Basically, there are two approaches: defining an own material or taking a predefined material with equal or rather adjustable characteristics.

Defining a User Defined Material (UMAT) was rejected due to the necessary time and effort. Nevertheless, the potential of creating an own material model was recognized.

The material used in the beginning was the MAT_CRUSHABLE_FOAM (MAT63). This material model was first used by Gagnon[14] and later by Kim[15] also for an ice compression simulation. After several simulations with the UMAT and a simple elastic material this foam analogue seemed to be a reasonable compromise between time consumption and practicability. Besides the usual variables for a material model a variable volumetric strain versus stress curve needs to be defined. Figure 3-2 shows the settings of the curve based on the relation generated by Kim. In terms of the relative volume V, the volumetric strain γ is defined as:

$$\gamma = 1 - V \tag{3.1}$$

The relation accounts for the cyclic hardening of the ice during a compression experiment. The jumps of the yield stress are forcing a typical saw-tooth pattern. From the material science perspective, the relation of yield stress and volumetric strain lacks physical interpretation because the volume of ice cannot change in the way defined. In fact, in the experiment there were only marginal density variations measured after the compression.

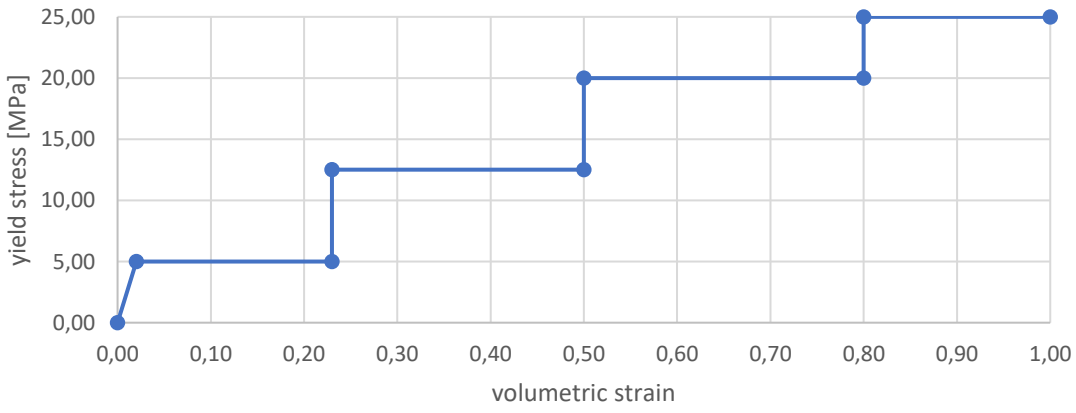

Figure 3-2: Volumetric Strain – Yield Stress relation of MAT63

In addition, a failure criterion is supposed to reflect the fracture of ice and generate the load drops recognized as the saw-tooth pattern of the normal force.

The results generated by the foam analogue were underestimating the measured values. Both the deviation in the results as well as the contradictions when analyzing the yield stress – volumetric strain relation, lead to the choice of an alternative. The material model MAT24 Piecewise Linear Plastic is widely applied in structural analysis to rate dependent simulations is. The material model offers a variable stress strain relationship. The characteristics assumed for the simulation of the ice in compression experiments are shown in Figure 3-3. The yielding of the material starts from the beginning at a stress of 1 MPa. From this point on the stiffness is discontinuously decreasing. The result is a smooth curve for the normal force that is applicable without a failure criterion. Obviously, this curve can only be used for a certain temperature and strain rate. For the strain rate the material model offers the application of more than one stress-plastic strain curve and a curve defining the strain rate scaling effect on the yield stress. The dependency on the strain rate would have implied that simplifications made concerning the velocity of the specimen would no longer be valid. For this reason, these options are not considered in this investigation.

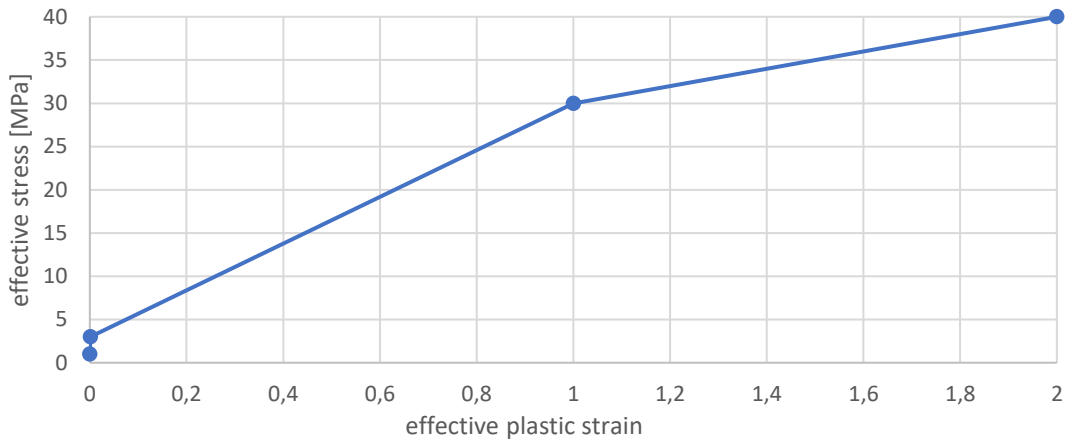

Figure 3-3:effective stress vs effective plastic strain of MAT24

The material model is also used in an only SPH simulation offering a good comparability of the two methods.

3.1.2 Failure Criteria

For the application in a combined FEM-SPH simulation an additional failure criterion is needed. Both in the MAT24 and in the MAT63 the failure criterion must be implemented with the additional keyword MAT_ADD_EROSION. There are different criteria which

can be applied even at the same time. Reasonable is the setting that only one criterion must be satisfied. The following criteria were investigated:

- MAXPRES – maximum pressure
- SIGVM – von Mises stress
- VOLEPS – volumetric strain

The von Mises stress seemed to be a reasonable criterion that causes the change of the material appearance observed during the experiment. It also takes the shear stress into account. It is practicable to observe the maximum stresses in the FEM calculation to get an idea of the extent of the deleted finite elements. Furthermore, it seemed reasonable to define a total stress cut off (constant stress with increasing plastic strain) for the SPH particles to avoid unphysical stress peaks. Pressure melting of ice starts at approximately 100 MPa at a temperature of -10°C and can therefore be set as the ultimate stress value [35].

3.1.3 Contact Definition

For each time step contact algorithms check the master segment (plate) for penetration by the slave segment (cylinder). When dealing with penalty based contacts the penetration is eliminated by applying a force proportional to the penetration depth. There are different penalty based contact algorithms that can also be used simultaneously. Experiences with different contact types shows that the computation time is increasing significantly when used at the same time. Furthermore, it can result in numerical instabilities. For these reasons, the investigations on the algorithms are concentrated on only one algorithm at one time. A simplified model is used and the maximum force, as well as the stress distribution, are compared to visualize the large variations resulting from different contact definitions. The contact algorithms investigated are briefly described in the following with respect to their application area [34].

- ERODING_NODES_TO_SURFACE - is recommended when solid elements are eroded – contact surface will be updated
- AUTOMATIC_NODES_TO_SURFACE - is recommended for the coupling of FEM and SPH elements - the slave part is defined with SPH and the master part is defined with finite elements

The simplified model consists of a cuboid discretized with finite elements and a solid to SPH option. A rigid plate is moving with a constant velocity onto the cuboid as visualized

in in Figure 3-4. The figure demonstrates the distribution of the von Mises Stress for three time steps.

NTS	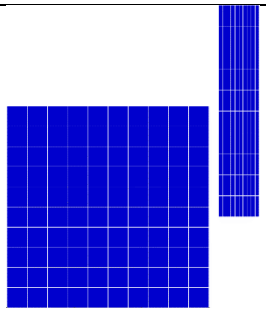	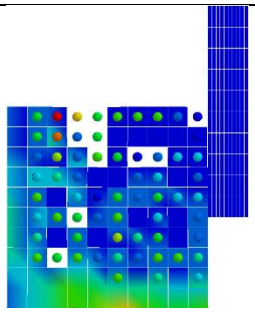	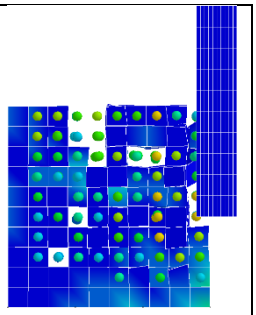
s [mm]	0	2,2	5
NTS-ER	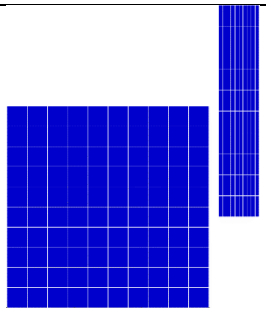	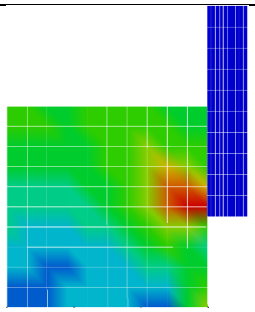	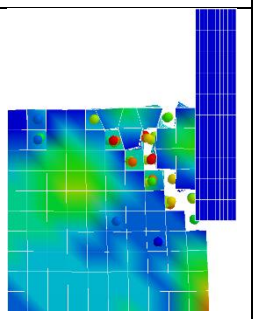
s [mm]	0	2,2	5

Figure 3-4: Animation for different contact options

For both the solid and the SPH part MAT63 is used as a material model. Two simulations are carried out with equal settings except the change of the contact definition of the solid parts. The contact in the first simulation (NTS) is realized by the Automatic Nodes to surface contact algorithm for both parts. In the second simulation (NTS-ER) the solid-solid contact is achieved by the Eroding Nodes to surface contact algorithm which is recommended for solid elements consisting a failure criterion. The computation time varies significantly - NTS-ER is 15 times slower. The resultant forces of the parts interacting with the plate are shown in Figure 3-5. In NTS the contribution on the force by the solid elements is relatively small. As soon as the contact occurs, it seems that elements are being deleted randomly throughout the cuboid. In contrast to this the force contribution of the solid elements in NTS-ER is significantly higher and the distribution of the von Mises stress displayed in Figure 3-4 seems physically more realistic. In both simulations the contact of the SPH part with the plate occurs with a certain gap. The gap results from the distance of the plate moving up to the center of the SPH particle as they are in the center of a solid element. This is an issue of the solid to SPH technique that is unavoidable.

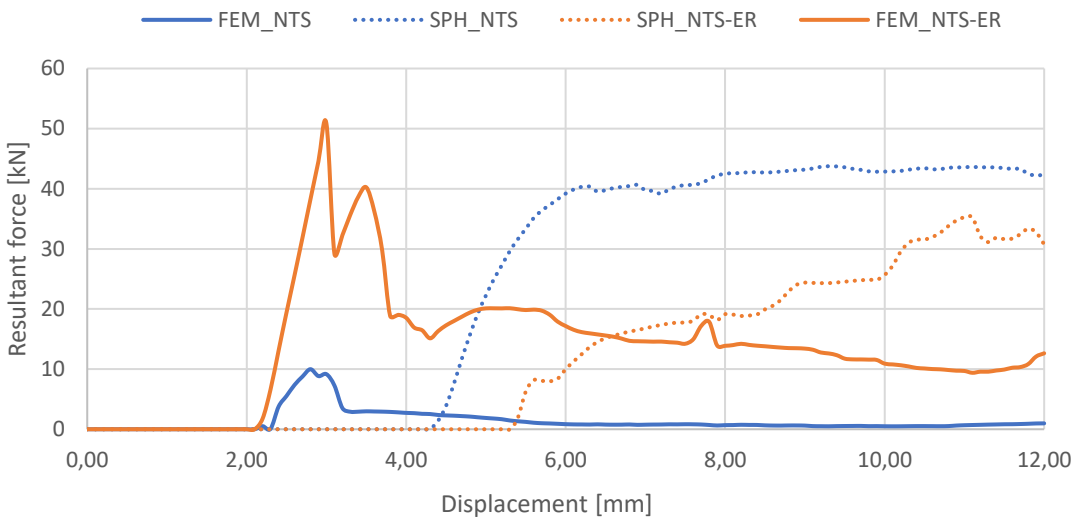

Figure 3-5: Forces on plate for different contact options

The contact algorithm used for further investigations is the AUTOMATIC_NODES_TO_SURFACE. This decision was made for the sake of simplicity. The condition can be used for both SPH-FEM and FEM-FEM contacts. More essential is the computation time which is 15 times larger for the ERODING_NODES_TO_SURFACE. This section focused on the large variations obtained from different contact definition and lead to the conclusion that results should always be treated with caution, especially when not every aspect is fully understood.

3.1.4 SPH Modifications

This section deals with the settings for the SPH part. First, some general settings are discussed and afterwards settings related to the combined simulation are depicted.

In the Keycard CONTROL_SPH the space dimension of the particles is set to a 3D problem. The smoothing function, which is essential for the particle approximation, is carried out each time step. It is set to a level that is recommended for most solid structure experiments. However, experience shows that changes of the default settings go along with significant increase of the computation time. Another crucial adjustment in this keycard is the activation of IEROD. This switch allows the application of a failure criterion for the SPH particles. The particles are not eliminated but the stress state is set to zero. The stress cut off is necessary to deal with unphysical stress peaks, as mentioned in section 3.1.1. To visualize the event the switch ISHOW can be activated, that transforms the particles to the default point visualization. To disable the contact, that is equivalent to a deletion of the particle, the switch ICONT can be activated.

There are different options when implementing SPH particles in a FEM calculation [see also Figure 3-6]. At first the number of particles that are being created from one solid element can be chosen. For a hexahedron element the options are 1, 8 or 27 particles. In contrast to an only SPH simulation the particles are always generated within the geometrical body of a finite element as shown in Figure 2-6. This leads to an unavoidable gap in the contact as discussed in Section 3.1.3. LS-DYNA provides different coupling methods between the particles generated for the failed elements and the remaining elements. Coupling can either take place when the solid element fails or from the beginning. Without any coupling it is called debris simulation. In this case a contact must be defined to prevent the generated particles from diffusing through the FEM mesh. These options were investigated with a simplified model. The debris simulation could not be successfully implemented as the particles still diffused through the mesh even with a contact condition defined. The two coupling options were most promising when the animation was analyzed in terms of the behavior of the particles and their stress distribution. As a matter of fact, the newly generated phase observed in the experiment is homogeneous and well connected to the solid ice phase. The difference between “coupling from beginning” and “coupling when element fails” was found to be negligible. For both options all the particles inherit the information of the finite elements right before failure. The contact forces of the SPH part are qualitatively similar. However, the contact force of the FEM part is significantly higher for the “coupling when element fails” option. In a simplified model the “coupling from beginning” option provided more stable results. For this reason, it was chosen for the final simulation. Nevertheless, these options should be investigated in more detail for further research on the combined simulation.

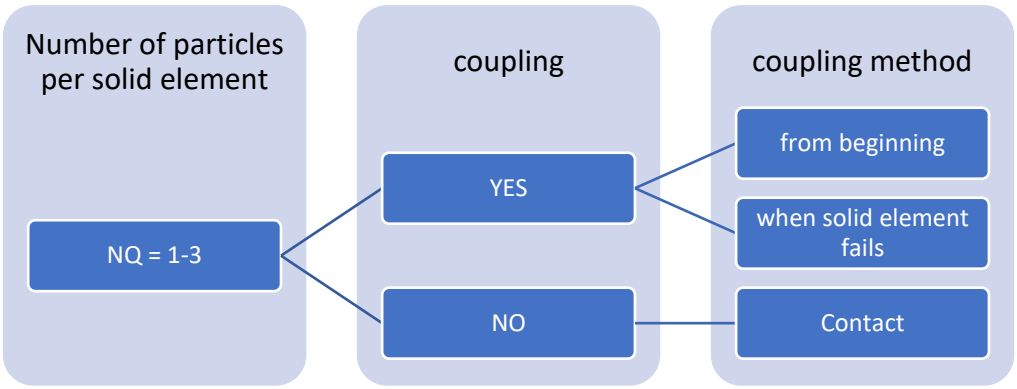

Figure 3-6: Options for ADAPTIVE_SOLID_TO_SPH

3.2 Experiment Set Up

The experiment was carried out to investigate the force and pressure of confined ice. In doing so, an ice specimen is pushed against a rigid plate with a constant. The specimen has the shape of a conically shaped cylinder. Figure 3-7 gives an impression of the set up before and after the compression.

Figure 3-7: Set up of the compression test (Model II)

To study the complex material behavior of ice in compression several measurement devices are installed. The force and the displacement of the piston that pushes the ice cone onto the plate is recorded. The temperature is recorded on the surface of the ice specimen or in the coldroom in which the small-scale experiment is carried out. The force and pressure distribution on the steel plate is measured by a "TekScan" sensor.

The experiment was carried out in two different scales. In the following Table 3-1 the characteristics of both models are given.

Table 3-1: Characteristics of the experiment

	Model I	Model II
Diameter	200 mm	800 mm
Cone angle	30°	30°
Feed rate	1 mm/s	1 mm/s
Temperature in the lab	-10 °C	Approx. 20 °C

As mentioned in section 2.1 the reproductivity of ice experiments is an issue. The ice properties are extremely sensitive to the production and a lot of effort has been put into the optimization of this process. The ice specimens are made of commercial available

crushed ice mixed with distilled water. The aim of this method is to obtain grained freshwater ice with reproducible properties. The cylinder is conically shaped to prevent scaling effects due to different contact surfaces at the beginning.

3.2.1 Mesh

A running FEM model is mandatory for a combined simulation. The first step is the spatial discretization of the problem domain. The ice cylinder is discretized by 8 node hexahedron elements. The ice specimen is moving with a constant velocity onto the rigid plate, discretized by shell elements. To avoid contact instabilities from the very beginning due to undetected interpenetrations, the mesh of the rigid part (plate) should not be coarser than the mesh of the deformable body (cylinder). Moreover, the impact on the computation time is small when refining a rigid body since there are no strain and stress calculations carried out. In the final simulation the material of the plate was changed to steel to achieve a more realistic pressure distribution.

Due to the conical shape the meshing of the cylinder is especially challenging. The automatically generated mesh results, in the vertical direction, in the same number of elements over the basic area of the cylinder and therefore causes large deviations of the element size. Regarding the combined simulation it is especially disadvantageous to have relatively large elements in the top of the cone. An essential part of automatic meshing is the angle of the cone which controls the height of the cylinder and correspondingly the number of element rows in the plane. The irregularity of the mesh can be best observed when cutting the cylinder as visualized in Figure 3-8. Nevertheless, this is as good as it could be realized with a specific given cone angle.

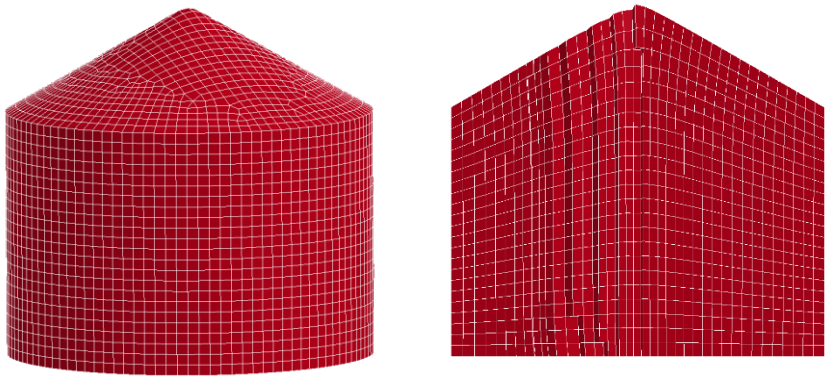

Figure 3-8: mesh of the large cone

Furthermore, the quality of a mesh depends on the size of the finite elements. Mesh refinements lead to an increase of the computation time. Therefore, the convergence of the

solution, in this case the maximum force, should be checked against the refinement of the mesh. In Table 3-2 and Figure 3-9 the outcome of a simple mesh study is presented. It shows a linear dependency of the computation time versus the number of elements and a convergence of the maximum force. The cone in the final simulation has about three times more elements compared to the one of the only FEM simulation 6_1_2.

Table 3-2: Net study

Simulation	6_1_0	6_1	6_1_2
elements/nodes	114/254	394/648	872/1386
relative part of elements	0,13	0,45	1
computation time	0,25	0,55	1
max z-force [N]	5250	3600	3250

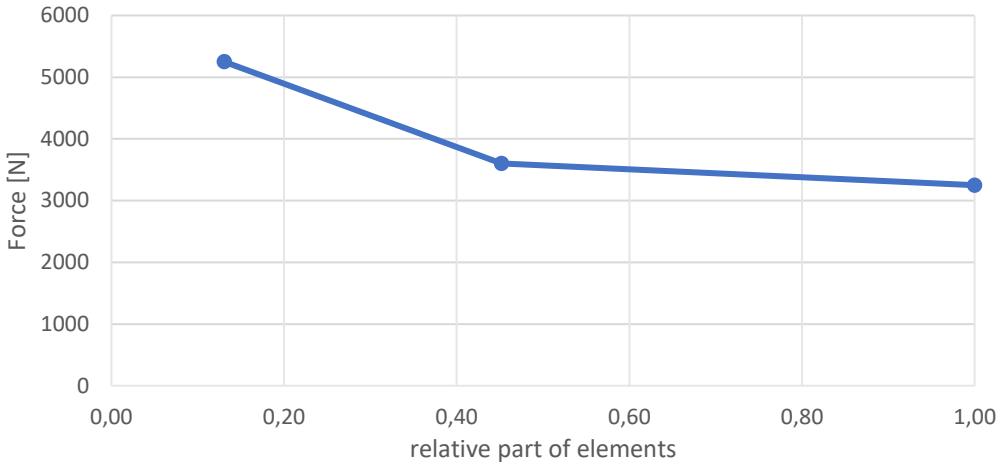

Figure 3-9: Net study

The mesh of the SPH particles is based on the mesh of the solid elements. For an only SPH simulation the particles can be created from the nodes of the solid elements. This gives the best results in terms of the replicability of the geometry's surface. For the combined simulation it is only possible to create the particles in or around the geometric center of a solid element. This results in 8% less solid elements and particles compared to the only SPH simulation.

In Figure 3-10 the bottom layer of all three meshes is shown. It can be noted that the SPH mesh is not as regular as recommended for the simulation [see also Figure 2-5].

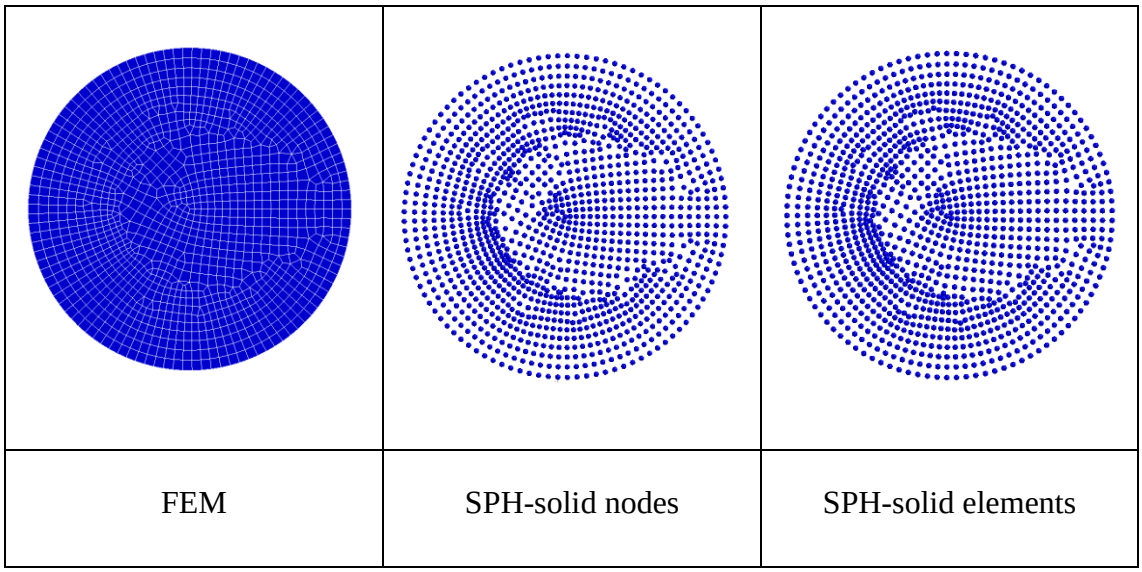

FEM	SPH-solid nodes	SPH-solid elements

Figure 3-10:comparison of FEM and SPH mesh

3.2.2 Boundary Conditions

The model is generated as simple as possible to minimize the sources of error. The cone is moving with a constant velocity of 100mm/s onto the plate which is fixed at its edges in all directions. The traverse speed is 100 times faster compared to the experiment. The computation time is decreasing proportionally due to the independency of the velocity on the calculated time steps during the integration. The explicit solver uses formula (2.1) to calculate the critical time step in a FEM simulation. The material models applied are independent from the strain rate and therefor this modification of the traversing speed is justifiable. The termination time corresponds to a penetration depth of 120 mm. The shell of the cylinder is fixed in all other than the direction of motion. This adjustment is essential to simulate the confinement of the ice. However, in the experiment the boundary conditions change due to the fact, that the cylinder is only guided for the length of the mould. This leads to an increasing boundary condition inaccuracy. Furthermore, the possible numerical inaccuracy and the increasing computation time lead to the premature termination. Furthermore, it needs to be mentioned that the boundary conditions are not inherit onto the particles when they are generated in the combined simulation.

3.3 Results

This section shows the outcome of the final simulations following the preliminary studies. Basically, the same numerical model is calculated using the FEM, SPH and the combined FEM-SPH method. The comparability of the results is guaranteed by keeping the settings for all numerical methods identical. For each simulation the results give the contact force,

the pressure distribution on the plate for specific time steps and a choice of numerical quantities.

3.3.1 Resultant Interface Force

The following figures display the resultant interface force on the plate versus the displacement of the ice specimen. This force is primarily acting in the direction of movement and results from the penalty based contact definition [see also section 3.1.3].

In Figure 3-11 the resultant forces of the three final simulations are compared. The force resulting from the only SPH simulation is on average 10 % smaller compared to the force resulting from the only FEM simulation. The curve of the combined FEM-SPH simulation fluctuates between the other curves and ends up with a force which is about the value of the FEM simulation.

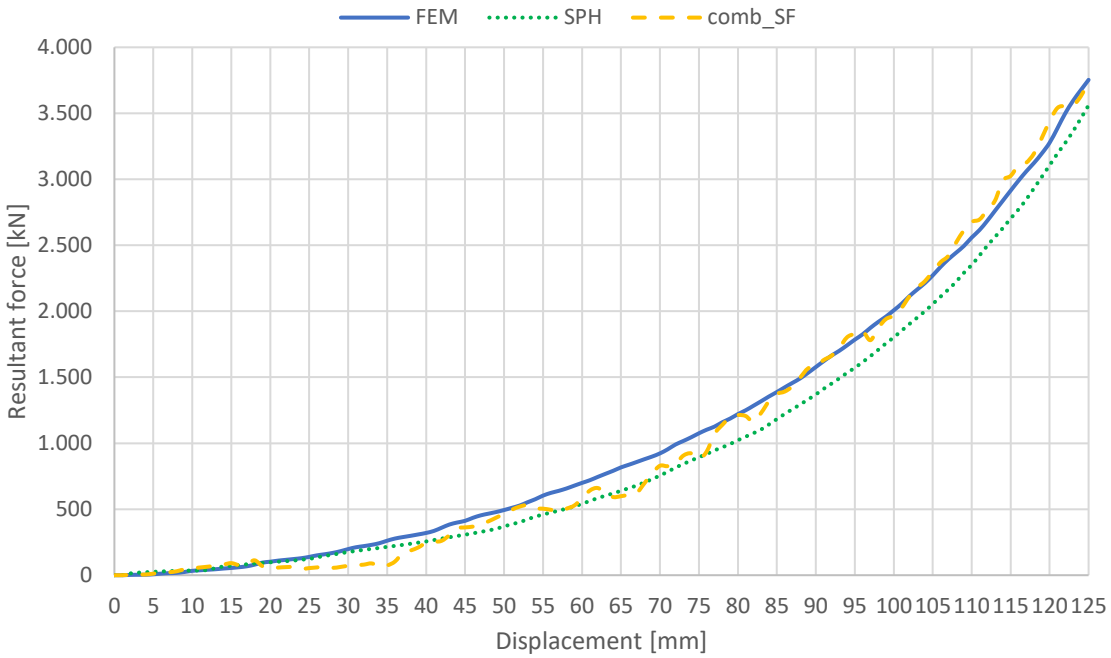

Figure 3-11: Resultant force of FEM, SPH and FEM+SPH simulation

The graph in Figure 3-12 shows the portions of the contact force of the combined simulation. The FEM-FEM contact force (FEM_SF) starts right at the beginning, increases slowly and stays at a value of roughly 250 kN. The SPH-FEM contact force (SPH_SF) starts with an offset of 35 mm and increases up to a value of 3500 kN at the final displacement of 125 mm. Both the SPH_SF and the FEM_SF show a course that is not smooth. The same applies to the combined resultant force (comb_SF).

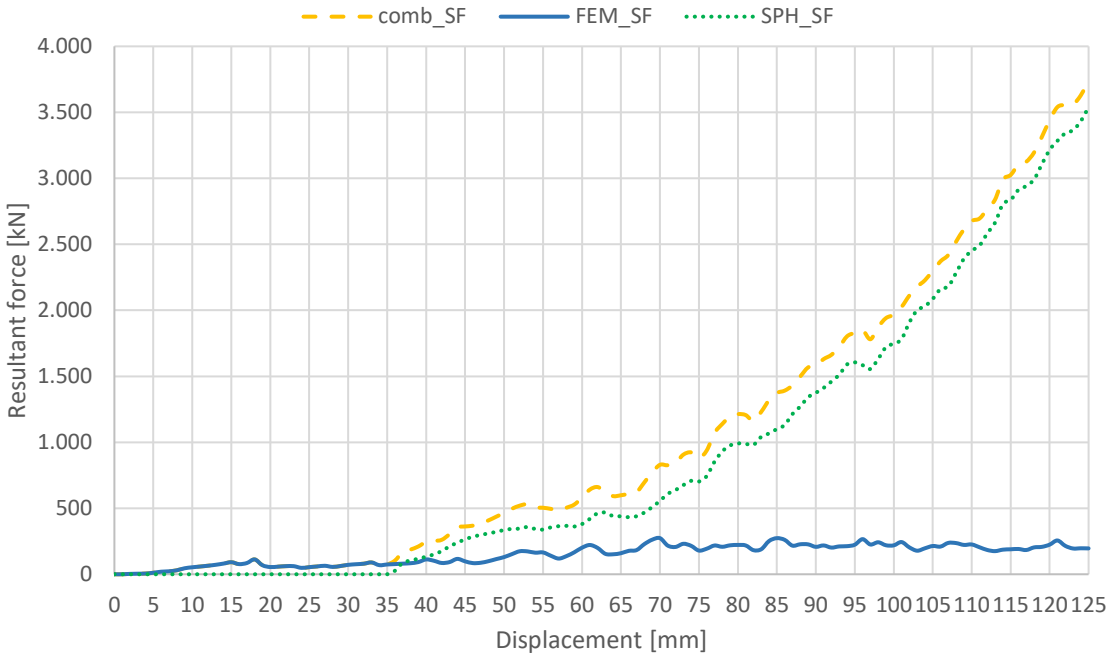

Figure 3-12: Resultant forces of the combined simulation

3.3.2 Pressure and Stress Distribution

The following figures display the pressure distribution recorded on the plate and the distribution of the von Mises Stress of the ice specimen. The figures are snapshots taken for two different time steps. The first one is at a displacement (s) of 15 mm which is just before the failure of the first element in the combined simulation. The second time step is at 90 mm. At this stage distortions of finite elements in the combined simulation start to develop. A scale next to the respective figures shows the range of the pressure/stress in MPa.

3.3.2.1 Displacement = 15 mm

Figure 3-13 visualizes the pressure distribution on the plate. Only the FEM snapshot shows symmetry. Furthermore, significant difference between the FEM and FEM-SPH snapshot should be noted.

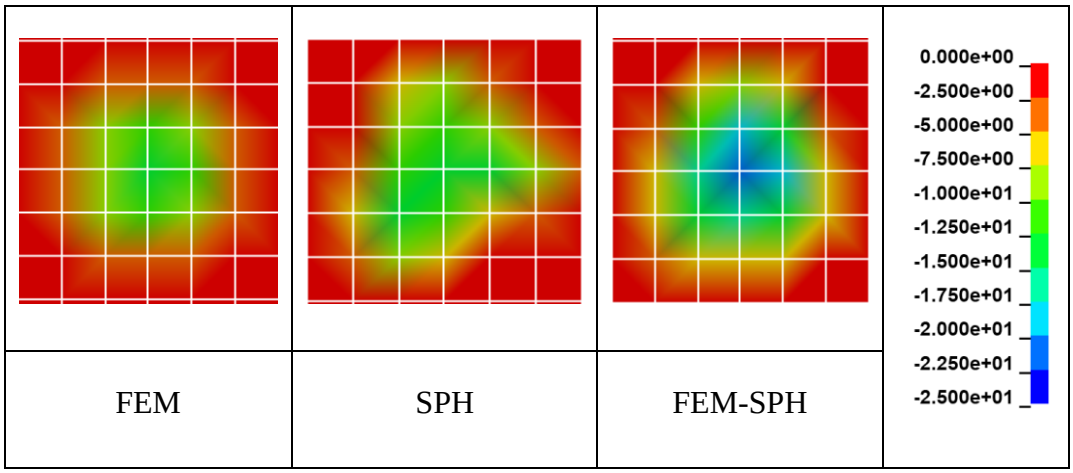

Figure 3-13:Interface Pressure [MPa] at s=15 mm

Figure 3-14 shows the distribution of the von Mises Stress on the shell of the cylinder. Both - the FEM and SPH simulation - show a centered downward distributed stress. Additionally, the cylinder of the combined simulation shows stress waves migrating through the structure.

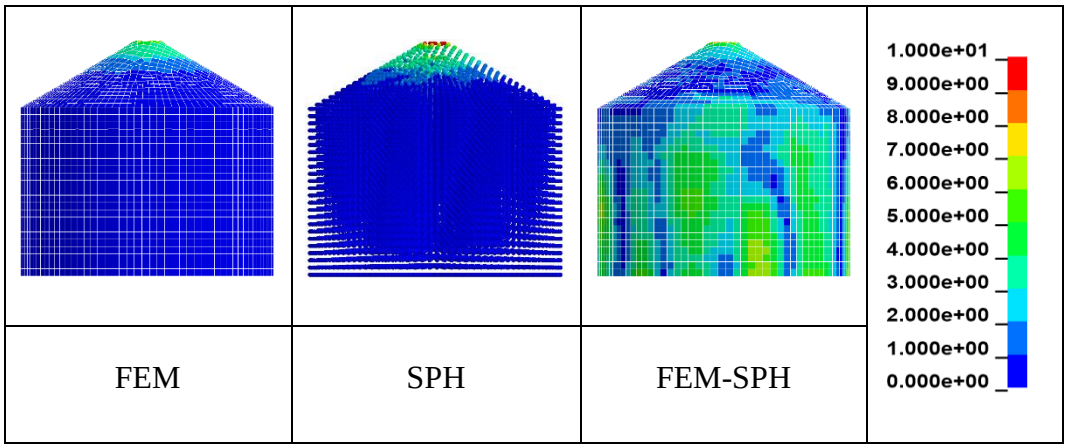

Figure 3-14:Von Mises Stress [MPa] at s=15 mm

3.3.2.2 Displacement = 90 mm

The pressure distributions in Figure 3-15 visualizes certain deviations: In comparison the FEM shows the highest values. The SPH simulation displays lower values but a greater extent of the area. The combined simulation has the smallest extent and in contrast to the FEM simulation small pressure values.

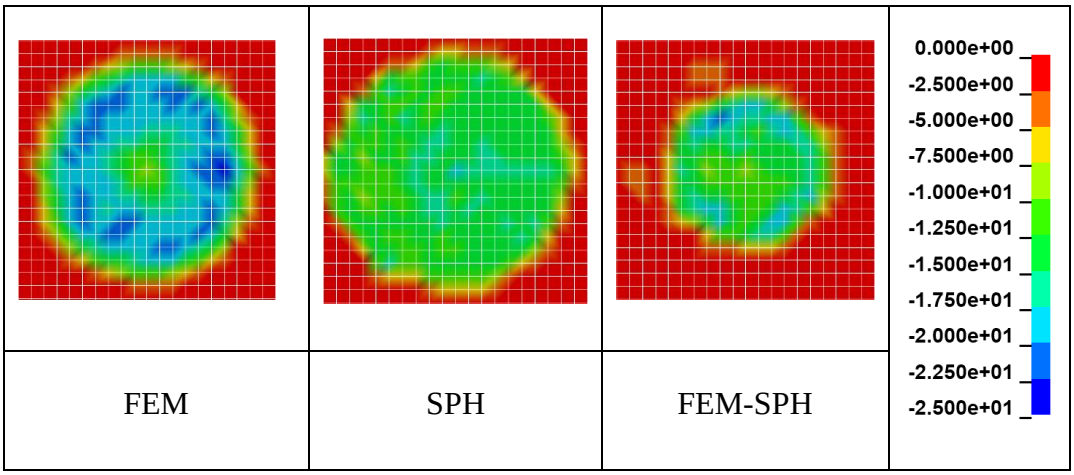

Figure 3-15:Interface Pressure [MPa] at s=90 mm

In Figure 3-16 the Interface pressure of the combined simulation was divided into the different parts acting on the plate. It should be noted that, compared to the finite elements, the proportion of the SPH particles is greater. Furthermore, in comparison to the middle snapshot, the pressure peaks are reduced in the combined snapshot.

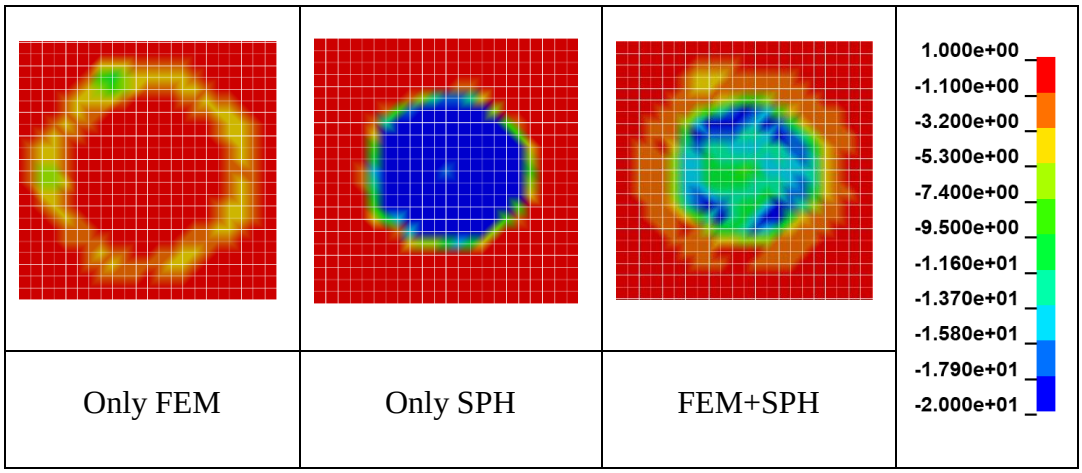

Figure 3-16:Interface Pressure [MPa] of the combined simulation at s=90 mm

The snapshots in Figure 3-17 show the Von Mises Stress of the blanked cylinder. The distribution of the stresses in the SPH and FEM simulation are comparable. The combined simulation displays a deviating pattern.

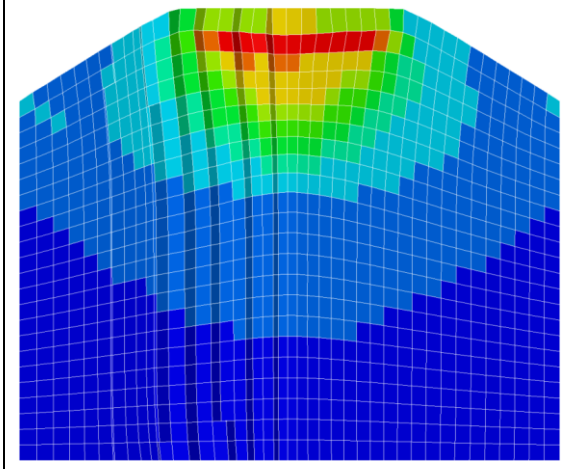

FEM

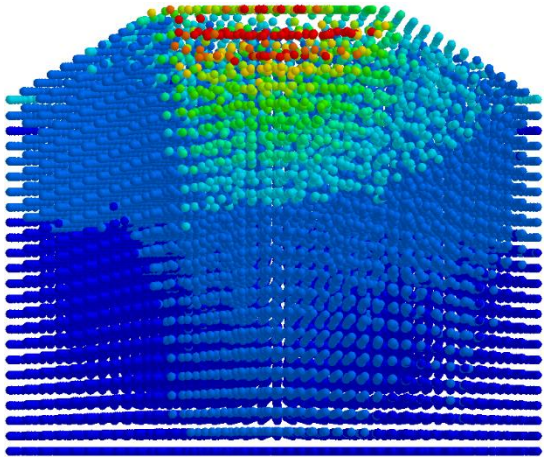

SPH

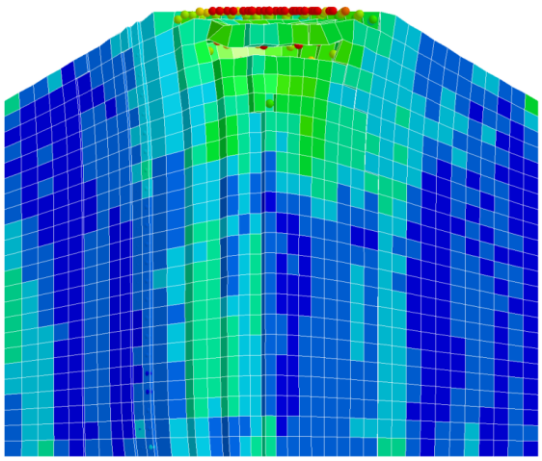

SPH-FEM

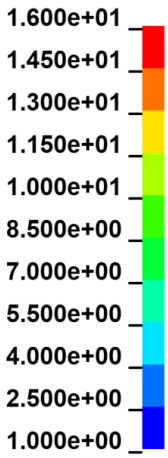

Fringe Level

Figure 3-17:Von Mises Stress [MPa] at s=90 mm

3.3.3 Numerical Aspects

The computation time is listed in Table 3-3 in relation to the time of the combined simulation. Compared to the combined simulation the FEM simulation is 20 times faster.

Table 3-3: General data

General Data	FEM	SPH	FEM-SPH
time [h]	2,92	38,20	76,63
proportional	1	13	26

The size of the time step is a central aspect of the explicit solver. Figure 3-18 displays the the time step size during the simulation. The SPH simulation has a constant offset. Both, the FEM and the combined simulation, demonstrate fluctuating time step offsets. Notable is the drop of the time step size in the combined simulation which starts at a displacement of 9 mm. The number of failed elements increases linearly.

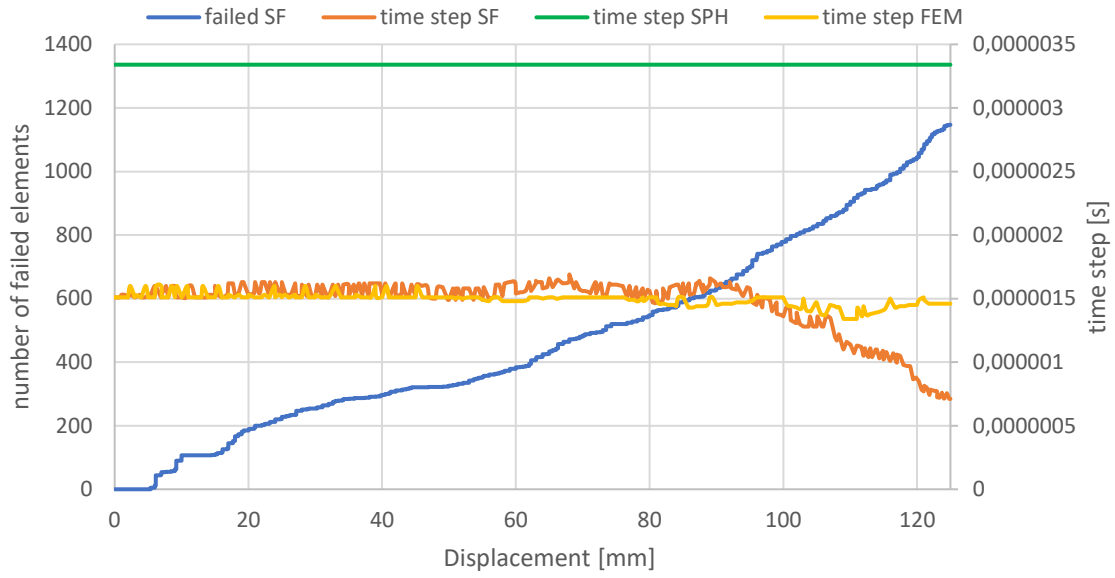

Figure 3-18: time step offset / failed elements versus the displacement

3.4 Discussion

The numerical studies are concluded with a discussion of the results. The focus of the discussion lies on the applicability and practicability of the combined simulation.

The resultant interface forces of all three simulations displayed in Figure 3-11 are correlating. Taking into consideration that one is dealing with fundamentally different approaches, this result is satisfactory in terms of the applicability of the alternative numerical methods. The choice of the smoothing function as well as the number of solid elements which is 8 percent lower compared to the number of particles could cause the constant difference between the SPH and FEM simulation. The fluctuation of the combined simulation can be derived with certainty from the failure of the solid elements. The load drop arises from the gap between the contact of the element and the contact of the particle. In Figure 3-12 the force of the combined simulation can be further analyzed. The animation indicates that the first elements on the shell fail at a displacement of 15 mm. From this moment on the FEM-FEM contact in the combined simulation shows an unsteady course. After the erosion of the top of the cone a small plateau can be seen. At this stage the SPH

particles are still not in contact with the plate. The first contact of the particles is recognized by the plate at a displacement of 35 mm. The SPH-FEM contact also shows an unsteady course not because the implemented stress cut off but due to the eroded elements in the core of the cylinder. Because the solid elements are continuously eroded the FEM-FEM contact force does not increase significantly.

The offset of the first FEM and the first SPH contact emphasizes an issue of the combined simulation. The SPH particles can only be generated in the center of the finite element. However, the contact is not recorded until the center of the particle meets the contact criterion in this case 20 mm after the failure of the elements in the tip. The particles inherit the stress state of the failed elements but lose the contact. Assuming a recrystallisation and not a fracture of the material, the loss of the contact in physically incorrect. The refinement of the mesh and an increase of the number of particles generated from one solid element can minimize but not solve this issue.

The behavior of the material can be described as ductile. The model offers a plastic strain of the ice analogue which was also observed in the experiment. The defined stress versus effective plastic strain curve (Figure 3-3) shows a linear course in the affected area below 30 MPa. The resultant interface forces of all three simulation display a similar course and can easily be approximated with a third-degree polynomial. This behavior is correlates with about the first half of the measurements. When comparing the results with data from a large-scale experiment (Figure 3-19), the curve of the forces demonstrates a similar course up to a displacement of about 55 mm. From this point on the experiment shows an irregularity resulting in a linear growth of the force. This pattern could also be adopted by the material model by adjusting the strain-stress curve. A decrease of the stress-strain curve in an earlier stage is imaginable. Furthermore, the option in the combined simulation is to use a different material model for the SPH part should be considered. In the sum the results produced by the material model are satisfactory in the context of the numerical investigation. From the material scientific perspective, the development of a user defined material is most promising in further research.

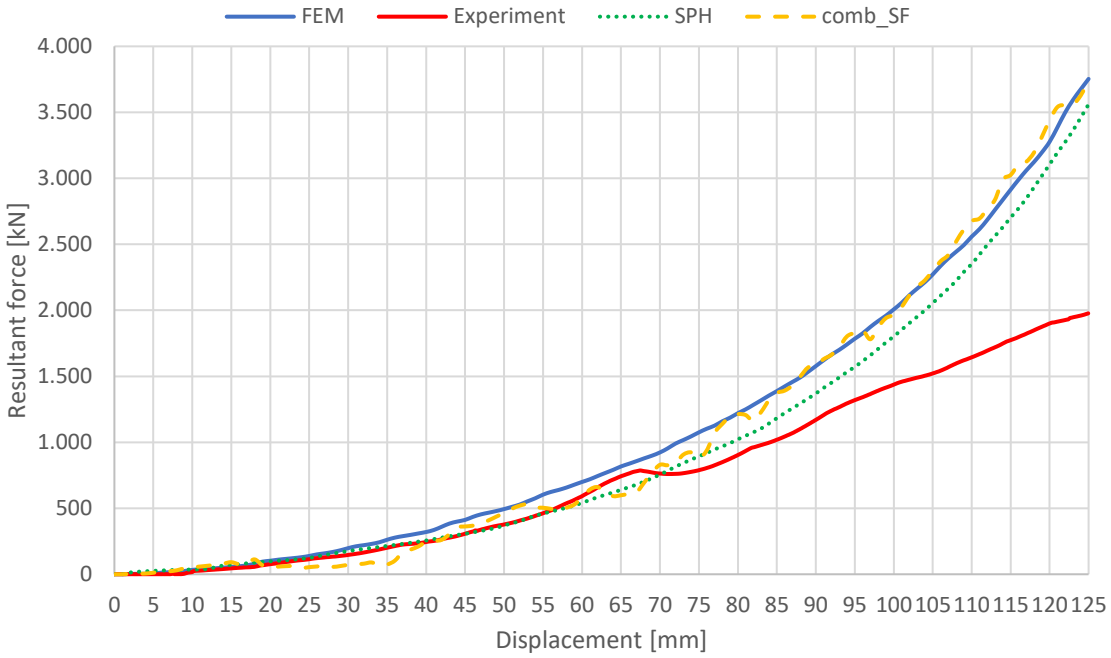

Figure 3-19: Simulation versus experiment

At a displacement of 15 mm only small contact forces are recorded and the differences between the simulations are hard to identify in the figures of the contact force. Even though in the combined simulation no elements have failed yet the pattern of the pressure distribution shown in Figure 3-13 differs significantly from the FEM simulation. This leads to the conclusion that the SPH particles are already affecting the behavior of the solid part and strengthen the structure in this case. The connection between the solid part and the particles should develop when the failure takes place. Otherwise, the method would falsify the results.

Another pattern only recognized in the combined simulation are stress waves visualized in Figure 3-14. There is no explanation yet for this unphysical behavior except the connection to the erosion criterion. The stress waves are continuously moving through the body even before any finite elements have failed. In an FEM simulation Lui et al. also observed stress waves but stated that they are generated after the erosion of elements. Instead of the failure criterion they adopted a material model and used plastic strain as a criterion for fracture [13]. In the combined simulation there is no other option but eroding elements and therefore accepting this numerical artifact.

The deviation of the pressure distribution of the combined and the FEM simulation continue even at a displacement of 90 mm. The contact force indicates that the distribution of the pressure, displayed in Figure 3-15, should look similar in sum but it shows a major

deviation. This phenomenon can be best explained by splitting up the pressure distribution of the combined simulation as shown in Figure 3-16. Both portions of the pressure distribution are partly eliminating each other. This leads to the conclusion that the plate is deforming in a way that affects the pressure distribution on the plate. A rigid material for the plate could solve this issue.

Finally, the von Mises Stress distribution inside the specimen shown in Figure 3-17 is worth an assessment. The FEM snapshot displays a regular distribution. The SPH snapshot is not as regular but demonstrates a similar pattern. The combined simulation still shows the stress waves mitigating through the structure. This even leads to the failure of finite elements outside the main stress area shown in the FEM snapshot. The failure criterion deletes finite elements that exceed a Von Mises Stress of 10 MPa. Consequently, stresses beyond the upper limit of 16 MPa are only generated by the particles.

The costliest simulation regarding the computation time is the combined simulation as shown in Table 3-3. The SPH method seems to be more complex in general. Even though the time step size is constantly only half of the size of the FEM simulation (Figure 3-18) the computation of the SPH simulation takes about 13 times longer. The time step size of the combined simulation is dominated by the solid elements (formula (2.1)). This might also be the reason for the even larger computation time – the SPH part is forced to calculate more time steps than necessary. In the beginning the curve of the time step size in the combined simulation shows the same pattern and similar values as the FEM simulation. The drop of the time step size at a displacement of 90 mm can best be explained with a significant increase of distortions in the finite elements. The number of failed elements does not influence the time step size, but it certainly affects the computation time.

4 Conclusion

Within this chapter the outcome of the numerical investigation on a combined FEM-SPH simulation is summed up. The practical approach of this project allows only a rather simple assessment and there are aspects that need to be investigated further. An outlook indicates possible aspects for future research.

Regarding the correlation of the contact forces the results of the final simulations presented in section 3.3.1 are satisfying. The ability to model the transformation of the material and to handle large deformation was proven for the combined simulation. The following particularities of the combined simulation were discussed:

- The Eroding option possibly leads to unphysical stress waves in the structure
- The application of two different material models in one simulation is possible
- The pressure distribution on the plate is possibly unphysical
- The time step size is smaller compared to the SPH simulation and the computation time is as a result 26 times higher compared to the FEM simulation

The preliminaries were regarding the innovative character of the combined simulation indispensable and lead to the following remarks:

- The contact options have a major effect on the outcome and the computation time
- The effect of the SPH particles on the structure before any element has failed and the gap of the contact are issues of the combined simulation
- The discretization of the cylinder is challenging and may result in certain irregularities
- The physical correctness of the material model (Crushable Foam) is doubtful

There are many different approaches for the numerical investigation of ice and yet there is not one method that can be seen superior, universal applicable or reliable. The results presented justify further investigation on alternative simulation methods with the focus on a user defined material model. To take full advantage of all the possibilities of a combined simulation the materials of the parts should differ. Different failure criteria could be applied to eliminate large distortions in the mesh.

5 References

[1] BMWi, “Eckpunkte für die Reform des EEG,” Federal Ministry for Economic Affairs and Energy, 2014.

[2] N. Schmelzer, J. Holfort, and P. Löwe, *Klimatologischer Eisatlas für die Deutsche Bucht (mit Limfjord): 1961-2010*. Hamburg und Rostock: Bundesamt für Seeschifffahrt und Hydrographie, 2015.

[3] W. Popko, J. Heinonen, S. Hetmanczyk, and F. Vorpahl, “State-of-the-art Comparison of Standards in terms of Dominant Sea Ice Loads for Offshore Wind Turbine Support Structures in the Baltic Sea,” *Proceedings of the International Offshore and Polar Engineering Conference*, 2012.

[4] M. Määttänen, “Ice induced frequency lock-in vibrations - Converging towards consensus,” *Proceedings of the International Conference on Port and Ocean Engineering under Arctic Conditions, POAC*, vol. 2015, 2015.

[5] L. Kellner, H. Herrning, and M. Ring, “Review of ice load standards and comparison with measurements,” in *Proceedings of the ASME 2017 36th International Conference on Ocean, Offshore and Arctic Engineering*, 2017.

[6] R. U. Franz von Bock und Polach and S. Ehlers, “On the Scalability of Model-Scale Ice Experiments,” *J. Offshore Mech. Arct. Eng*, vol. 137, no. 5, p. 51502, 2015.

[7] T. S. Nord, O. Øiseth, and E.-M. Lourens, “Ice force identification on the Nordströmsgrund lighthouse,” *Computers & Structures*, vol. 169, pp. 24–39, 2016.

[8] D. Molybeux, D. Spencer, and L. Liu, “Loads due to first year ice ridges on a vertical cylinder,” in *Proceedings of the ASME 2013 32nd International Conference on Ocean, Offshore and Arctic Engineering*, 2013.

[9] A. Munjiza, J. Paavilainen, J. Tuhkuri, and A. Polojärvi, “2D combined finite-discrete element method to model multi-fracture of beam structures,” *Engineering Computations*, vol. 26, no. 6, pp. 578–598, 2009.

[10] Hilding, Daniel and Forsberg, Jimmy and Arne Gürtner, Dr, “Simulation of ice action loads on off shore structures,” in *Proceedings of the 8th European LS-DYNA Users Conference*, 2011.

[11] P. F. Moore, I. J. Jordaan, and R. S. Taylor, “Explicit finite element analysis of compressive ice failure using damage mechanics,” in *Proceedings of the 22nd International Conference on Port and Ocean Engineering under Arctic Conditions,* 2013.

[12] Z. Lui, J. Amdahl, and S. Loset, “Integrated numerical analysis of iceberg collisions with ship sides,” in *Proceedings of the 21st International Conference on Port and Ocean Engineering under Arctic Conditions*, 2011.

[13] Z. Lui, J. Amdahl, and S. Loset, “Numerical simulation of collisions between ships and icebergs,” in *Proceedings of the 20th International Conference on Port and Ocean Engineering under Arctic Conditions*, 2009.

[14] R. E. Gagnon, “A numerical model of ice crushing using a foam analogue,” *Cold Regions Science and Technology*, vol. 65, no. 3, pp. 335–350, 2011.

[15] K. Hyunwook, “Simulation of Compressive "Cone-Shaped" Ice Specimen Experiements using LS-DYNA,” in *Proceedings of the 13th International LS-DYNA Users Conference*, 2014.

[16] I. J. Jordaan, J. Xiao, J. Wells, and A. Derradji-Aouat, *Ice crushing and cyclic loading in compression*, 2008.

[17] M. B. Liu and G. R. Liu, “Smoothed Particle Hydrodynamics (SPH): An Overview and Recent Developments,” *Arch Computat Methods Eng*, vol. 17, no. 1, pp. 25–76, 2010.

[18] M. H. Keegan, D. Nash, and M. Stack, “Numerical modelling of hailstone impact on the leading edge of a wind turbine blade,” Vienna, 2013.

[19] T. J. Sanderson, *Ice mechanics: Risks to offshore structures*. London: Graham & Trotman, 1988.

[20] G. W. Timco and W. F. Weeks, “A review of the engineering properties of sea ice,” *Cold Regions Science and Technology*, vol. 60, no. 2, pp. 107–129, 2010.

[21] E. M. Schulson and P. Duval, *Creep and Fracture of Ice*. Cambridge: Cambridge University Press, 2009.

[22] S. Brandslet and A. S. Midling, *Crushing Ice to Save Offshore Structures.* [Online] Available: http://www.maritime-executive.com/blog/crushing-ice-to-save-offshore-structures. Accessed on: Sep. 19 2017.

[23] J. J. Petrovic, “Review Mechanical properties of ice and snow,” *Journal of Materials Science,* vol. 38, no. 1, pp. 1–6, 2003.

[24] Alexander Vill, “Ice-Properties and Preperation of Ice-Structure-Interaction-Specimens,” Bachelor Thesis, Institut für Konstruktion und Festigkeit von Schiffen, TUHH, 2016.

[25] G.-R. Liu, *Meshfree methods: Moving beyond the finite element method,* 2nd ed. Boca Raton, Fla.: CRC Press, 2010.

[26] B. Klein, *FEM: Grundlagen und Anwendungen der Finite-Element-Methode im Maschinen- und Fahrzeugbau,* 6th ed. Wiesbaden: Vieweg+Teubner Verlag, 2005.

[27] Prof. Dr.-Ing. habil. Alexander Düster, *Strukturanalyse von Schiffen und meerestechnischen Konstruktionen: Vorlesungsskript 2013/2014*, 2013.

[28] John O. Hallquist, “LS-DYNA Theory Manual,” 2006.

[29] R. A. Gingold and J. J. Monaghan, “Smoothed particle hydrodynamics: Theory and application to non-spherical stars,” *Monthly Notices of the Royal Astronomical Society*, vol. 181, no. 3, pp. 375–389, 1977.

[30] L. B. Lucy, “A numerical approach to the testing of the fission hypothesis,” *The Astronomical Journal*, vol. 82, p. 1013, 1977.

[31] G. R. Liu and M. B. Liu, *Smoothed particle hydrodynamics: A meshfree particle method*. Singapore: World Scientific, 2005.

[32] W. Benz and E. Asphaug, “Simulations of brittle solids using smooth particle hydrodynamics,” *Computer Physics Communications*, no. 87, pp. 253–265, 1995.

[33] Livermore Software Technology Corporation (LSTC), “LS-DYNA KEYWORD USER'S MANUAL: VOLUME I,” 2016.

[34] Livermore Software Technology Corporation (LSTC), *dynasupport.com.* [Online] Available: http://www.dynasupport.com/tutorial/contact-modeling-in-ls-dyna. Accessed on: Dec. 07 2017.

[35] W. Wagner, T. Riethmann, R. Feistel, and A. H. Harvey, “New Equations for the Sublimation Pressure and Melting Pressure of H 2 O Ice Ih,” *Journal of Physical and Chemical Reference Data*, vol. 40, no. 4, p. 43103, 2011.